Experimental and Theoretical Study of a Low-Pressure Axisymmetric Arcjet

J.N. Le Toulouzan,* G. Gouesbet,† R. Darrigo,‡ and A. Berlemont§
Institut National des Sciences Appliquées, Rouen, France

An experimental study of a helium plasma axisymmetric arcjet has been conducted. The laminar and compressible He jet flows in a low-pressure ($p = 130$ Pa), ambient-temperature, helium gas at rest. Pressure measurements using static and differential pressure probes were carried out. The temperature is measured at one point from the analysis of the Boltzmann equilibrium between rotation levels. A numerical integration of the jet governing equations leads to the prediction of the pressure, temperature, and velocity fields. A modified version of the TEACH-L computer program is used. The comparison between predictions and experiments is very satisfactory.

I. Introduction

THE plasma under examination in this study is a helium axisymmetric arcjet flowing in a low-pressure, ambient-temperature helium at rest. The experimental measurements concern pressure data obtained with a (differential) pressure probe, and the gas temperature at a single point deduced by analyzing the Boltzmann equilibrium between rotation levels. Special care was taken in the interpretation of pressure probe measurements to take into account the influence of thermal, viscous, and rarefaction effects.[1-5] Ideally, direct velocity measurements should have been obtained, and there were two possible techniques for this. The determination of Doppler shift in emission spectra[6-9] was not attempted because it required high-spectroscopy techniques that were not readily available in the laboratory. Laser-Doppler anemometry (LDA)[10-16] was attempted but was not successful, although some data had been produced in a previous investigation[17] of a low-pressure, high-temperature situation.

This is one of the reasons why the jet parameter profiles were predicted by numerical integration of the governing equations (Navier-Stokes, continuity, and energy). The dissipation of mechanical energy into heat, usually neglected, is taken into account in this paper. These predictions were found to be in good agreement with the experimental results for differential pressures.

Despite the problem involved in obtaining a complete description of the flow, there is nevertheless a general interest in jet computations, especially under plasma conditions.[18-24]

II. The Plasma Torch

The plasma is a 6-kW helium laminar arc produced between an anode and a cathode and blown out of a nozzle. The helium specification is He U (fewer than 50-ppm impurities). The gas-injection volume flow rate is equal to 20 l/mn and kept constant within 1%. The diameter of the nozzle exit is $\phi_d = 20$ mm. The arc voltage is 25 V, $\pm 0.2\%$, and the arc current 250 A, $\pm 2\%$.

The axisymmetric flow is blown into a low-pressure chamber where the static pressure is equal to 130 Pa and kept constant within 3%. The chamber is equipped with two windows for optical investigations, which also enable us to verify the correct running of the plasma. The low pressure is obtained by means of a pumping group resting on a concrete block isolated from the ground by antivibration supports and linked to the test chamber by a metallic expansion joint. The test chamber also rests on a concrete block with antivibration supports. More details are given by Le Toulouzan.[25]

III. Measurements

Pressure Measurements

Let p_1 and p_2 be the static pressures on both sides of the impact-pressure probe shock wave, respectively, upstream and downstream of the flow, and let p_{O2} be the impact pressure downstream from the shock-wave front. We measure a differential pressure Δp equal to the difference between the impact pressure p_{O2} given by the impact probe and the static pressure p_1 given by a static-pressure probe, located in the test chamber, outside the jet:

$$\Delta p = p_{O2} - p_1 \tag{1}$$

The double pressure probe for differential pressure Δp measurements is an optoelectronic device described in Fig. 1. There are three main parts: a Mylar film, an optical reflection detector (HEDS 1000, Hewlett Packard), and a quartz tube. The Mylar membrane divides the device into two chambers, the impact-pressure chamber and the static-pressure chamber. The difference Δp between the impact and the static pressures produces a deformation of the membrane that is detected by an optoelectronic device involving the optical detector and an electronic system.

The output signal from the electronic system is proportional to the differential pressure Δp. Calibration is carried out before the device is used in the plasma jet. As mentioned before, the static pressure outside the jet (measured by a Pirani probe) is kept constant within 3%. Furthermore, the static pressure in the jet is assumed to be constant and equal to the static pressure outside the jet.

The dynamic Δp range is 500 Pa, the spatial resolution about 1 mm, and the rise time less than 4 s. The error is less than 10-20% for Δp, depending on the location of the probe in the jet.

A point of concern is the influence of viscous and rarefaction effects,[4,5] which disturb the pressure measurements. From the described predictions,[4,5] the error between the measured impact pressure and the true impact pressure is estimated to be at worst 10% (in the far nozzle region) and has not been considered sufficiently important to be accounted for.

Received July 23, 1985; revision received March 31, 1986.

*Maître Conférences.
†Professeur. Member AIAA.
‡Professeur.
§Chargé de Recherches, C.N.R.S.

Principle of Gas-Temperature Measurements

The principle of gas-temperature measurements is based on the strong coupling between translation and rotation levels of energy, produced by collisions of the kind[26,27]

$$He_2^*(p,v,J) + He \rightleftharpoons He_2^*(p,v,J-2) + He \tag{2}$$

where p, v, J represent electronic, vibration, and rotation levels, respectively. Following Deloche et al.,[26] we assume that the gas temperature is equal to the rotational temperature of the electronic level $He_2 e^3\pi_g^-$. Assuming that all the rotation levels of any molecular species, for a given electronic level and a given vibration level, are coupled by the Boltzmann equilibrium, a rotational line intensity I_{em} is given by[28]

$$I_{em} = C\nu^4 S_J F_{vJ} \exp(-E_r/kT_r) \tag{3}$$

The subscripts are defined as follows: em is emission, C is a constant, ν the wavenumber of the transition, S_J the rotational line strength of the lower level J, F_{vJ} a correcting factor due to vibration-rotation interactions,[29,30] E_r the rotational energy of the upper level, k the Boltzmann constant, and T_r the rotational temperature of the molecular kind.

We studied the $e^3\pi_g^- - a^3\Sigma_u^+$ (0 – 0) He_2 transitions and plotted log $[I_{em}/(\nu^4 S_J)]$ vs E_r, where I_{em} is measured and ν, S_J, and F_{vJ} are calculated.

To determine T_r, the values of E_r, the rotational line strength S_J, and the wavenumber ν must be calculated for each J in the transition.

The rotational energy is given by

$$E_r = B_v J(J+1) \tag{4}$$

with

$$B_v = B_e - \alpha_e(v + \tfrac{1}{2}) \tag{5}$$

where B_e and α_e are rotational constants corresponding to the upper level and given by Herzberg.[28]

The rotational line strength S_J is deduced from Schadee expressions,[31] valid for $e^3\pi_g^- - a^3\Sigma_u^+$ (0 – 0) He_2 transitions

$$P_1 \text{ branch: } S_J = S_P(J) = J(2J+1)/6(2J-1) \tag{6}$$

$$Q_1 \text{ branch: } S_J = S_Q(J) = (2J+1)(J+1)(J-1)/6J^2 \tag{7}$$

The rotation line wavenumbers and wavelengths are computed with the following formulas:

$$\nu_P = \nu_0 + (B_v' - B_v'')J^2 - (B_v' + B_v'')J \tag{8}$$

$$\nu_Q = \nu_0 + (B_v' - B_v'')(J^2 + J) \tag{9}$$

with $\nu_0 = 21507.3$ cm^{-1}, where B_v' and B_v'' are the rotational constants corresponding to the upper- and lower-levels, respectively.

The Spectroscopy Device

The spectroscopic system used to measure the line intensities is based on a Huet monochromator with a 1.25-m focal length spherical mirror used in a Czerny-Turner mode. This spectroscopy device is also described in Ref. 32. All the measurement results corresponding to Sec. III will be given later.

IV. Numerical Predictions

Assumptions

Numerical predictions are carried out in a cylindrical coordinate system r, θ, z, where the radial, tangential, and longitudinal velocities are designated by u, v, and w, respectively. The following conditions are assumed:

1) The plasma jet is steady, axisymmetric, and laminar, and the fluid is compressible. It is a freejet flowing in a quiescent atmosphere.

2) The ionization rate is low ($\sim 7.10^{-4}$, according to Ref. 32). Consequently, the energies associated with recombination processes, emitted radiation, and electric fields are neglected.

3) The fluid is a perfect gas.

4) There are no abrupt variations in the properties of the plasma jet. Experimental results have shown that the plasma jet undergoes a transition between supersonic and subsonic regimes. Nevertheless, we did not observe any luminous discontinuity in the plasma jet. This led us to assume that the regime transition did not give rise to an abrupt shock wave but rather to a continuous process, probably because of the large mean free path of molecules. Consequently, the model neglects any abrupt variations in the plasma jet properties.

5) The tangential velocity v is zero.

6) The axial derivatives are much smaller than the radial ones.

$$\frac{\partial^2 u}{\partial z^2} \ll \frac{\partial^2 u}{\partial r^2} \tag{10}$$

$$\frac{\partial^2 w}{\partial z^2} \ll \frac{\partial^2 w}{\partial r^2} \tag{11}$$

Governing Equations

With the preceding assumptions, the relevant governing equations[33] reduce to

Navier-Stokes equations

$$u\frac{\partial(\rho u)}{\partial r} + w\frac{\partial(\rho u)}{\partial z} = -\frac{\partial p}{\partial r} + \frac{\partial^2(\mu u)}{\partial r^2} + \frac{\partial}{\partial r}\left(\frac{\mu u}{r}\right) \tag{12}$$

$$u\frac{\partial(\rho w)}{\partial r} + w\frac{\partial(\rho w)}{\partial z} = -\frac{\partial p}{\partial z} + \frac{\partial^2(\mu w)}{\partial r^2} + \frac{1}{r}\frac{\partial(\mu w)}{\partial r} \tag{13}$$

where μ is the dynamic viscosity of the fluid.

Continuity equation

$$\frac{\partial(\rho u)}{\partial r} + \frac{\rho u}{r} + \frac{\partial(\rho w)}{\partial r} = 0 \tag{14}$$

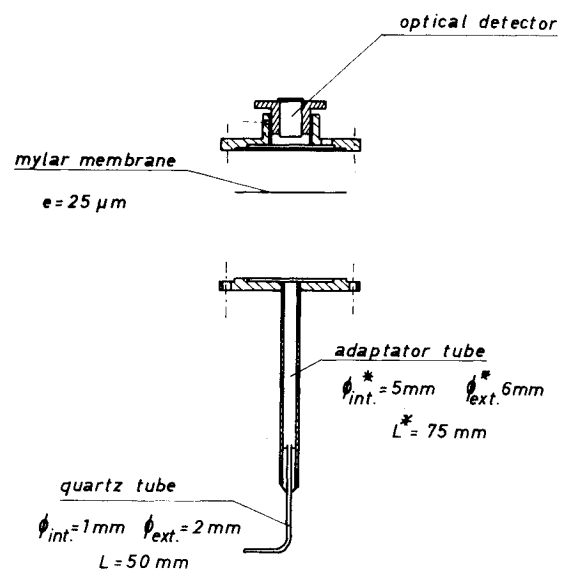

Fig. 1 Optoelectronic pitot probe.

Energy equation

$$u\frac{\partial(\rho C_p T)}{\partial r}+w\frac{\partial(\rho C_p T)}{\partial z}=\frac{1}{r}\frac{\partial}{\partial r}\left[r\frac{\partial(kT)}{\partial r}\right]+\left[\frac{\partial(\mu^{1/2}w)}{\partial r}\right] \tag{15}$$

where C_p is the heat capacity at constant pressure. The last term on the right-hand side of Eq. (15) represents the dissipation of mechanical energy into heat and is usually neglected in other works.

These equations are supplemented by an expression governing the dependence of the dynamic viscosity on temperature, according to:[34]

$$\mu/\mu_0=(T/T_0)^{0.67} \tag{16}$$

where T_0 is the temperature of the helium at rest surrounding the jet, equal to 293 K, for which $\mu=1.9614\ 10^{-5}$ kg·m^{-1}s^{-1} (Ref. 35).

Resolution of the Equation Set

The equation set is solved using a modified version of the TEACH-L computer program from the Imperial College of Science and Technology.[36] The following points must be mentioned:

1) The flow is assumed to be parabolic, so it exhibits a predominant direction (without any recirculation), all diffusive processes in that direction can be neglected, and the downstream pressure field has no influence on the upstream flow. It is thus possible for the computer program to use a marching integration procedure, from one upstream station to the next one downstream, and so on, the required fields, such as velocities and pressure, being calculated at each step. Sweeping in the z direction is not necessary.

2) The balance equations are solved by a cell finite difference scheme.

3) The algorithm SIMPLE is used for the pressure terms.[37]

4) The solution of the governing systems of linearized equations is obtained by the tridiagonal matrix algorithm (TDMA).[38]

5) An expanding grid (in the r direction) is introduced into the computer program (the expanding factor is equal to 0.15 or 0.21).

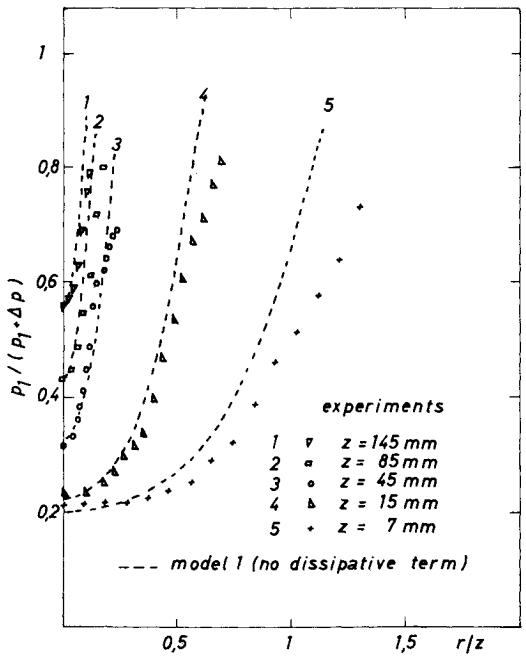

Fig. 2 Radial distributions of the ratio $p_1/p_1+\Delta p$: comparison between experiments and model 1.

To perform the marching procedure, inlet values are required. The inlet section for the numerical predictions, $z=0$, corresponds to the exit of the divergent nozzle.

Due to the increase in the size of the grid in the integration domain in the z direction, the results corresponding to the higher values are not significantly influenced by initial conditions. The longitudinal inlet velocity profile is assumed to be parabolic and the radial inlet velocity is equal to zero. The inlet temperature profile is given by

$$T=T_{\max} \qquad r<\phi_d/4$$

$$T=T_{\min} \qquad \phi_d/4<r<\phi_d/2 \tag{17}$$

Although these initial assumptions are somewhat arbitrary, the velocity and temperature profiles are interdependent and governed by the necessity that the mass flux conservation be preserved. The values retained are $T_{\max}=1100$ K, $T_{\min}=900$ K, and a longitudinal velocity on the axis equal to 2050 m/s.

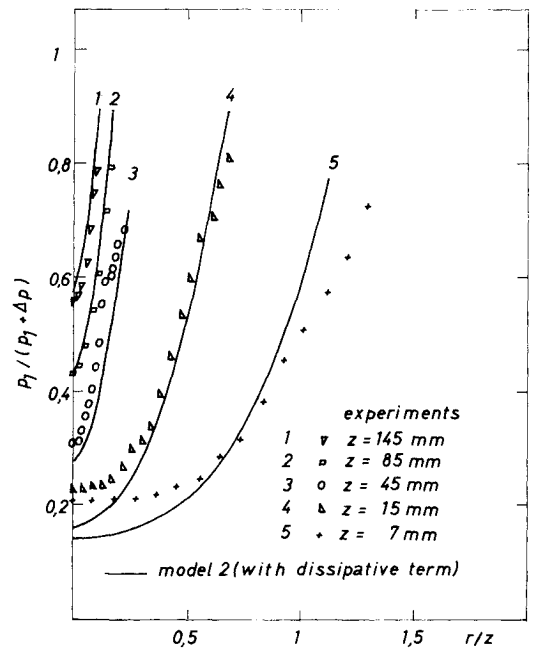

Fig. 3 Radial distributions of the ratio $p_1/p_1+\Delta p$: comparison between experiments and model 2.

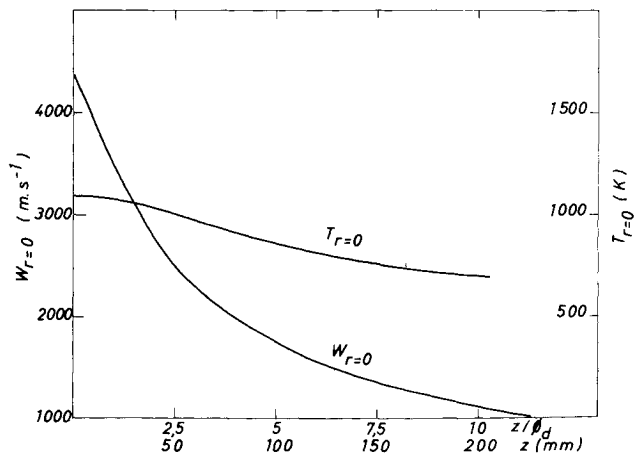

Fig. 4 Axial distribution of temperature and velocity from model 2.

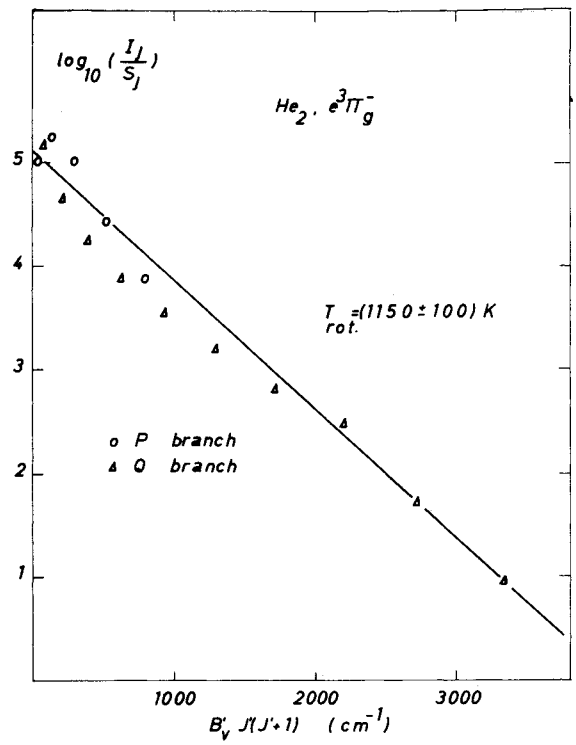

Fig. 5 Rotational line intensities I_J divided by the corresponding line strength S_J plotted vs rotational energy.

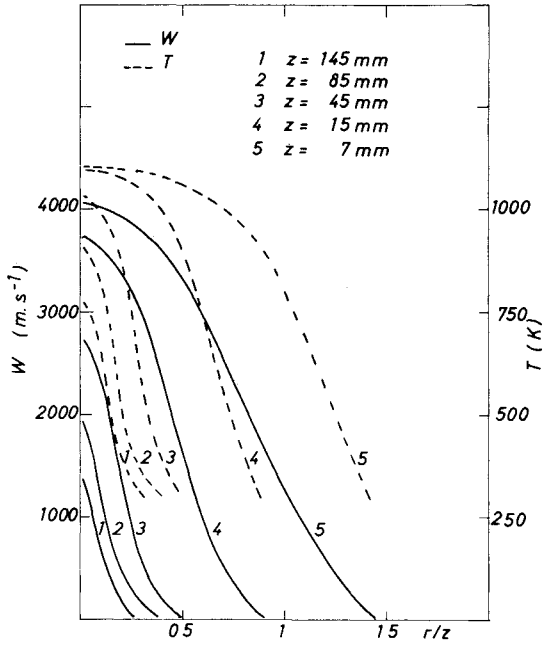

Fig. 6 Radial distributions of temperature and velocity from model 2.

V. Results and Discussion

The influence of the dissipative term in the energy equation can be discussed on the basis of Figs. 2-3. Figures 2 and 3 show the profiles $[p_1/(p_1+\Delta p)]$ vs r/z for several values of z. Two cases are considered: model 1, where the dissipation term is neglected, and model 2, where it is included in the energy equation. There is a significant difference between computed profiles using either model 1 or model 2, showing that the dissipative term cannot be neglected from a purely computational point of view. We conclude, however, that both models agree (reasonably) with experiments, especially when we take into account the experimental errors and the assumptions present in the computation models, which also lead to model inaccuracies. From now on however, model 2 will be used because, as the dissipative term does exist, it is more physically realistic.

In Fig. 3, the agreement between model 2 and experiments is nearly perfect for $z>45$ mm. For $z<45$ mm, the difference remains smaller than 30%, increasing as the nozzle exit is approached. This discrepancy is mainly attributed to the fact that, in this region, the flow characteristics are significantly dependent on initial conditions. In fact, the assumed inlet profiles are expected to be different from the true profiles.

For 80 mm $<z<150$ mm (profiles 1 and 2), the agreement between model 2 and experiments is better than 2% on the axis and 6% on the edges. In this far region, the agreement is very satisfactory. Initial conditions have been found to influence these results, but although the figures should therefore be modified, the qualitative conclusions remain the same. For instance, with $T_{max}=1200$ K and $T_{min}=800$ K, agreement is obtained within 3% on the axis and 8% on the edges.

The longitudinal profiles of the longitudinal velocity w for $r=0$ and temperature T for $r=0$, taken from model 2, are shown in Fig. 4. As mentioned, no experimental results have been obtained for the velocities, and experimental results for the temperatures concern only the section $z=15$ mm for $r=0$. The model leads to $T_{r=0}$ ($z=15$ mm) equal to ~ 1050 K, while experiments led to 1150 ± 100 K (Fig. 5). This agreement is very satisfactory. However, it is not that significant since it depends on the chosen values for the inlet temperature profiles. From Fig. 4, it can be seen that the Mach number ranges from 2 near the nozzle exit down to 0.7 for $z\sim 200$ mm, confirming the passage from a supersonic to a subsonic regime as discussed previously. Finally, radial profiles of w and T are given in Fig. 6 at various z values.

VI. Conclusion

Measurements of pressures and of a single-point temperature have been carried out in a helium plasma axisymmetric arcjet flowing in a low-pressure, ambient-temperature helium gas at rest. Pressure, temperature, and velocity profiles have been predicted by means of a numerical integration of the governing equations. The dissipation of mechanical energy into heat, usually neglected, is taken into account. The experiments and the numerical predictions compare very satisfactorily. The conclusion is that numerical computations of plasma quantities in low-pressure, high-velocity arcjets are well suited to a priori predictions of plasma designs and should become routine practice.

Acknowledgments

The authors wish to thank J.C. Lecordier, U.A. CNRS No. 230, Rouen, and P. Savary, Laboratoire Génie Chimique Analytique, Institut National des Sciences Appliquées, Rouen, for help in the measurements.

References

[1]Grey, J. and Jacobs, P. J., Experiments on Turbulent Mixing in a Partially Ionized Gas," *AIAA Journal*, Vol. 2, March 1964, pp. 433-438.

[2]Hare, A. L., "Velocity Measurement in Plasma Flows Using Cooled Pitot Tubes. An Unsolved Problem," 3rd International Symposium on the Chemistry of Plasmas, University of Limoges, France, July 1977, IUPAC Communications.

[3]Yamamoto, K., "Impact Pressure Probe in Free Molecular Flow," *AIAA Journal*, Vol. 16, Nov. 1978, pp. 1181-1184.

[4]Cogan, D. M. and Harvey, J. K., "Probe Interference in High-Speed Rarefied Flows," *AIAA Journal*, Vol. 11, Dec. 1973, pp. 1765-1766.

[5]Peterson, C. W. and George, O. L., "Wind Tunnel Pressure Probes: New Calibrations for New Geometries and Flow Environments," *AIAA Journal*, Vol. 13, Oct. 1975, pp. 1263-1264.

[6]Ahlborn, B. and Barnard, A. I., "Velocity Measurement by Doppler Effect," *AIAA Journal*, Vol. 4, June 1966, pp. 1136–1137.

[7]Cambray, P., "Mesure de vitesse dans les jets de plasmas comportant des gradients axiaux," 3rd International Symposium on the Chemistry of Plasmas, University of Limoges, France, July 1977, IUPAC Communications.

[8]Vervisch, P., "Etude de la cinétique d'un plasma d'argon basse pression au voisinage d'une paroi," Thèse de Docteur-ès-Sciences Physiques, Rouen, France, March 1978.

[9]Cambray, P., "Contribution à l'étude de processus de relaxation dans les jets de plasma d'hélium à basse pression," Thèse de Docteur-ès-Sciences Physiques, Poitiers, France, 1980.

[10]Gouesbet, G. and Trinite, M., "Anémométrie laser-Doppler interférentielle dans une torche à plasma haute fréquence," *Journal of Physics E*, Vol. 10, 1977, pp. 1009–1016.

[11]Gouesbet, G., Valentin, P., and Grehan, G., "Laser Velocimetry in rf Plasmas," *Proceedings of International Workshop on Laser Velocimetry in Hostile Environments*, Purdue University, School of Mechanical Engineering, July 11–13, 1978, pp. 335–346.

[12]Gouesbet, G. and Grehan, G., "Laser-Doppler Systems for Plasmas Diagnostics: A Review and Prospective Paper," 4th International Symposium on Plasma Chemistry, Zurich, Aug. 1979.

[13]Krasovskjs, V. V. and Palagashvili, E. I., "Possible Application of the Laser Doppler Velocimeter to the Determination of Particle Velocities in Heterophase Plasma Flows Obtained Using Electric Arc Plasmatrons," *High Energy Chemistry (USSR)*, Vol. 13, No. 3, May-June 1979, pp. 236–239.

[14]Vardelle, A., Vardelle, M., Baronnet, J. M., and Fauchais, P., "Mesure des vitesses et des températures des particules de diametre donné injectées dans un jet de plasma d'arc," Revue Internationale des Hautes Températures et des Réfractaires, Vol. 17, 1980, pp. 221–233.

[15]Lesinski, J., Mizera-Lesinska, B., Jurewicz, J., and Boulds, M. I., "Particle and Gas Velocity Measurements in a d.e. Plasma Jet," Plasma Chemical Processing of the 88th AICRE National Meeting Philadelphia, PA, June 1980.

[16]Gouesbet, G., "A Review on Measurements of Particle Velocities and Diameters by Laser Techniques, with Special Emphasis on Thermal Plasmas," Plasma Chemistry and Plasma Processing, Vol. 5, No. 2, 1985, pp. 91–117.

[17]Garo, A., Puechberty, D., Gouesbet, G., and Ledoux, M., "Determination of Velocity Profiles Above a Thin Flat Plate in a Low Pressure Flame," *Letters in Heat and Mass Transfer*, Vol. 7, July-Aug. 1980, pp. 275–281.

[18]Abramovich, G. N., *The Theory of Turbulent Jets*, MIT Press, Cambridge, MA, 1963, pp. 3-11.

[19]Pai, S. I., *Fluid Dynamics of Jets*, D. Van Nostrand Co., New York, 1954.

[20]Schlichting, H., *Boundary Layer Theory*, 4th ed., trans. J. Kestin, Mc-Graw Hill, New York, 1960.

[21]Pack, D. C., "Laminar Flow in an Axially Symmetrical Jet of Compressible Fluid, Far from the Orifice," *Proceedings of the Cambridge Philosophical Society*, Vol. 50, 1954, pp. 98–104.

[22]Mazza, A. and Pfender, E., "Modeling of an Arc Plasma Reactor for Thermal Plasma Synthesis," *Proceedings of the 6th International Symposium on Plasma Chemistry*, Montreal, Quebec, Canada, July 1983, pp. 41–50.

[23]Correa, S. M., "Transitional Plasma Jet Modeling," *Proceedings of the 6th International Symposium on Plasma Chemistry*, Montreal, Quebec, Canada, July 1983, pp. 77–82.

[24]Wei, D., Correa, S. M., Apelian, D., and Paliwal, M., "Melting of Powder Particles in a Plasma Jet," *Proceedings of the 6th International Symposium on Plasma Chemistry*, Montreal, Quebec, Canada, July 1983, pp. 83–89.

[25]Le Toulouzan, J. N., "Plasmas He et He-K: Diagnostics, forces d'oscillateur de KI et coefficient de recombinaison de He_2^+," Thèse de Docteur-es-Sciences Physiques, Rouen, June 1983.

[26]Deloche, R., Monchicourt, P., Cheret, M., and Lambert, F., "High-Pressure Helium Afterglow at Room Temperature," *Physical Review A*, Vol. 13, No. 3, 1976, pp. 1140–1176.

[27]Brout, R., "Rotational Energy Transfer in Hydrogen," *Journal of Chemical Physics*, Vol. 22, 1954, pp. 934–939.

[28]Herzberg, G., *Molecular Spectra and Molecular Structure, I. Spectra of Diatomic Molecules*, 2nd ed., Van Nostrand Reinhold Co., New York, 1950.

[29]Ayoub, S. E., "Détermination du facteur d'interaction vibration—rotation pour les transtion $E^1\pi_g - A^1\Sigma_u^+$ et $e^3\pi_g^- - a^3\Sigma_u^+$ de la molécule He_2, Application à la mesure de la température de rotation," Thèse Doctorat, 3e cycle, Lyon I, July 1977.

[30]Chevaleyre, J., Bouvier, A., Ayoub, S., and Janin, J., "Determination of the Vibration-Rotation Integration Factor for Dihelium Transitions," *Journal of Physics B*, Vol. 11, No. 7, 1978, pp. 1227–1233.

[31]Schadee, A., "The Formation of Molecular Lines in the Solar Spectrum," B. A. N., Vol. 17, No. 5, March 1964, pp. 311-357.

[32]Le Toulouzan, J. N., Locquet, J. I., Allano, D., Savary, P., and Darrigo, R., "Inversion d'Abel d'un plasma cylindrique d'hélium. Réalisation d'un spectrographe stigmatique à détecteur VIDICON," *Journal of Optics of Paris*, Vol. 12, No. 6, 1981, pp. 369-376.

[33]Bird, R. B. and Stewart, W. E., *Transport Phenomena*, edited by N. Lightfoot, John Wiley & Sons, New York, 1960.

[34]*Handbook of Chemistry and Physics*, 56th ed., CRC Press, Inc., Cleveland, OH, 1975.

[35]Kestin, J. and Leidenfrost, W., "Absolute Determination of the Viscosity of Eleven Gases over a Range of Pressures," *Physica*, Vol. 25, 1959, pp. 1033-1062.

[36]Gosman, A. D. and Ideriah, F. J. K., *TEACH-L*, Department of Mechanical Engineering, Imperial College, London, 1976.

[37]Patankar, S. V. and Spalding, D. B., "A Calculation Procedure for Heat, Mass and Momentum Transfer in Three Dimensional Parabolic Flows," *International Journal of Heat and Mass Transfer*, Vol. 15, 1972, pp. 1787-1806.

[38]Scarborough, J.B., *Numerical Mathematical Analysis*, The Johns Hopkins Press, Baltimore; Oxford University Press, London, 1966.